Hindawi
Advances in Civil Engineering
Volume 2021, Article ID 6679333, 11 pages
https://doi.org/10.1155/2021/6679333

Research Article

Experimental Study on the Effect of Brittleness on the Dynamic Mechanical Behaviors of the Coal Measures Sandstone

Junce Xu,[1] **Hai Pu**,[1,2] **and Ziheng Sha**[1]

[1]*State Key Laboratory for Geomechanics & Deep Underground Engineering, China University of Mining & Technology, Xuzhou, Jiangsu 221116, China*
[2]*College of Mining Engineering and Geology, Xinjiang Institute of Engineering, Urumqi, Xinjiang 830091, China*

Correspondence should be addressed to Hai Pu; haipu@cumt.edu.cn

Received 23 December 2020; Revised 27 January 2021; Accepted 4 February 2021; Published 17 February 2021

Academic Editor: Zhijie Wen

As one of the most crucial mechanical parameters of the rock materials, the effect of brittleness on the deformation and failure is of great practical significance for geotechnical construction and disaster prevention and mitigation. In this paper, the deformation and failure behaviors of the different brittle samples under dynamic loading were investigated using a split Hopkinson pressure bar (SHPB) experimental system. Besides, scanning electron microscopy (SEM) was also employed to study the relationship between the microscopic failures and rock brittleness and strain rate effects. The results revealed that the brittleness indexes BI_3 and BI_5 of the samples under uniaxial compression follow a linearly decreasing trend affected by the temperature changes, while the brittleness of the sample shows an increasing trend with the increase of strain rate under the dynamic loading. Also, the decline in the brittleness leads to an increase in the prepeak yield deformation phase of the sample under dynamic loading; after the peak point, the sample failure mode transitions from type I to type II with self-sustaining failure. Moreover, it was found that the dynamic strength increase factor presents a negative correlation with the sample brittleness. Finally, the macroscopic failure mode of the sample changes from split failure with multiple cracks to shear failure with few cracks due to the effect of decreasing brittleness. The failure surface of the sample gradually becomes smooth with the increase of brittleness, which manifests as a decrease in microcracks, and the gradual increase of the strain rate makes the failure surface rough, accompanied by an increase in microcracks.

1. Introduction

Brittleness is an essential parameter of rock materials that can describe the process of rock deformation and failure [1, 2]. An insightful understanding of the changes in rock brittleness is essential to the design and development of rock engineering systems, such as stability for deep mining roadway, excavation for underground space, the selection for shale gas reservoirs, etc. [3, 4]. Rock burst phenomenon in underground mining engineering is also closely related to the brittleness because it is a key parameter for determining the occurrence and possibility of rock burst [5–7]. Overall, brittleness is a comprehensive description of rock mechanical behavior [8, 9]. Therefore, considering the influence of rock brittleness has certain guiding significance for the development of various rock projects.

There are different views on the definition of rock brittleness at home and overseas. Some scholars argued that the effect of changes in environment and stress state on rock brittleness should not be considered since brittleness is an intrinsic property of rocks related to mineral composite and texture composition. Jarvie et al. and Rickman et al. believed that the rock brittleness is related to mineral components, especially the content of brittle minerals such as quartz and feldspar [10, 11]. Jin et al. and Rybacki et al. concluded that the rocks with a high content of strong/brittle minerals exhibit higher brittleness, while a large number of weak/ductile minerals (like clay) would reduce the brittleness of

rocks [12, 13]. However, different external factors, such as moisture content, temperature, etc., inevitably lead to changes in brittle state and failure mode of rock materials. Xia et al. and Li et al. considered that the variations in rock mechanical parameters, such as strength, elastic modulus, and Poisson's ratio, would inevitably lead to variations in rock brittleness [14, 15]. Moreover, based on the cyclic freeze-thaw experimental results in the lab, Zhang et al. explored the influence of freeze-thaw action on the sandstone brittleness, and the results revealed that the freeze-thaw effect had a clear impact on rock brittleness [16]. Therefore, when evaluating the change of rock brittleness, the internal and external conditions, like temperature, stress state, and microstructure, should be comprehensively considered. For instance, the mechanical behavior of rocks changes significantly with the increase of mining depth in mining engineering. Particularly, after the rock excavation, the stress release changes the microstructure and mechanical properties of the surrounding rocks, which may vary the surrounding rock brittleness. However, these phenomena always are ignored in mining activity.

To quantify the rock brittleness variation, the concept of the brittleness index was proposed. So far, no internationally accepted standard has been defined for the determination of rock brittleness index [17]. At present, there are mainly several ways to estimate the rock brittleness index: mineral composition, rock strength, strain parameters, stress parameters, and energy balance. Moreover, Heidari et al. believed that the porosity affects the brittleness of the rock, and they found that the increase in porosity would induce an increase of plastic strain at failure and finally reduces the rock brittleness [18], while this brittleness index based on porosity values shows contradictory results due to the neglect of diagenesis. Besides, Nejati and Ghazvinian verified that the variation in rock brittleness has a significant impact on the damage evolution of rocks under dynamic loading [19], but they only qualitatively analyzed several rock samples with different brittleness and did not quantify the results with brittleness indexes. At present, there are many researches on the brittleness of different kinds of rocks [20]. However, many studies focus too much on how to describe the brittleness of rock materials and ignore the influence of rock brittleness on mechanical behavior, especially under dynamic loading conditions. Therefore, it is necessary to study the response of rocks to brittleness change under dynamic loading.

To investigate the influence of brittleness on the dynamic mechanical behavior of the coal measures sandstone, in this paper, the brittleness index was first determined using the stress-strain curves. Subsequently, dynamic impact experiments were performed on the different brittle sandstone samples with a split Hopkinson pressure bar (SHPB) experimental system. Further, the effect of brittleness on macro- and microfailure characteristics was studied by a high-speed camera and a scanning electron microscope (SEM). Finally, the research results can provide reference significance for the construction of deep rock engineering, such as mining and tunnel projects.

2. Materials and Experimental Methods

2.1. Samples Preparation. This study used coal measures sandstone collected from a roof of a working face in Sanhejian Coal Mine, Xuzhou, China (see Figure 1). Mineralogy and petrological properties of the sandstone selected were studied via X-ray Diffraction (XRD), and the results revealed that the sandstone contains a large amount of quartz, as well as a small amount of kaolinite, chlorite, berlinite, and nacrite. All the tested samples were taken from the same large and relatively complete sandstone block, and the cores of rock were drilled in the same direction. The diameter of each sandstone samples was processed into 50 mm, and the ratio of length to diameter was 2 and 1 for static and dynamic tests, respectively [21]. To reduce the uncertainty of the experimental results, the samples were screened out before the tests: first, the samples with visible defects were eliminated, and then an ultrasonic P-wave test was used to remove the samples with internal defects (only the samples with P-wave velocities of 3200 ± 100 m/s were selected). Finally, a total of 18 and 30 sandstone samples for static and dynamic tests, respectively.

2.2. Determination of Brittleness Index (BI). As described in Section 1, the rock brittleness can be quantitatively characterized by different methods. We summarized five main methods to define the rock brittleness parameter in Table 1. Among these definitions of rock brittleness, considering the characteristics of stress-strain curves to determine rock brittleness is the most effective and reasonable method [28]. As shown in Figure 2, there are several key parameters for determining rock brittleness based on the characteristics of stress-strain curves [13]. In this study, to facilitate the analysis, the BI_3 and BI_5 from equation (1) were chosen to evaluate the samples brittleness:

$$\begin{cases} \mathrm{BI}_3 = \dfrac{\varepsilon_e}{\varepsilon_p}, \\ \mathrm{BI}_4 = \dfrac{\left(\varepsilon_r - \varepsilon_p\right)}{\varepsilon_p}, \\ \mathrm{BI}_5 = \dfrac{\left(\sigma_p - \sigma_r\right)}{\sigma_p}, \\ \mathrm{BI}_6 = \dfrac{\sigma_r}{\sigma_p}, \end{cases} \tag{1}$$

where σ_p and σ_r refer to peak strength and residual strength, respectively; ε_e, ε_p, and ε_r are the elastic strain, peak strain, and residual strain, respectively.

Due to the influence of excavation activities, the surrounding rocks of underground engineering would be damaged in different degrees, especially deep mining activities. At the same time, the variation in surrounding rock

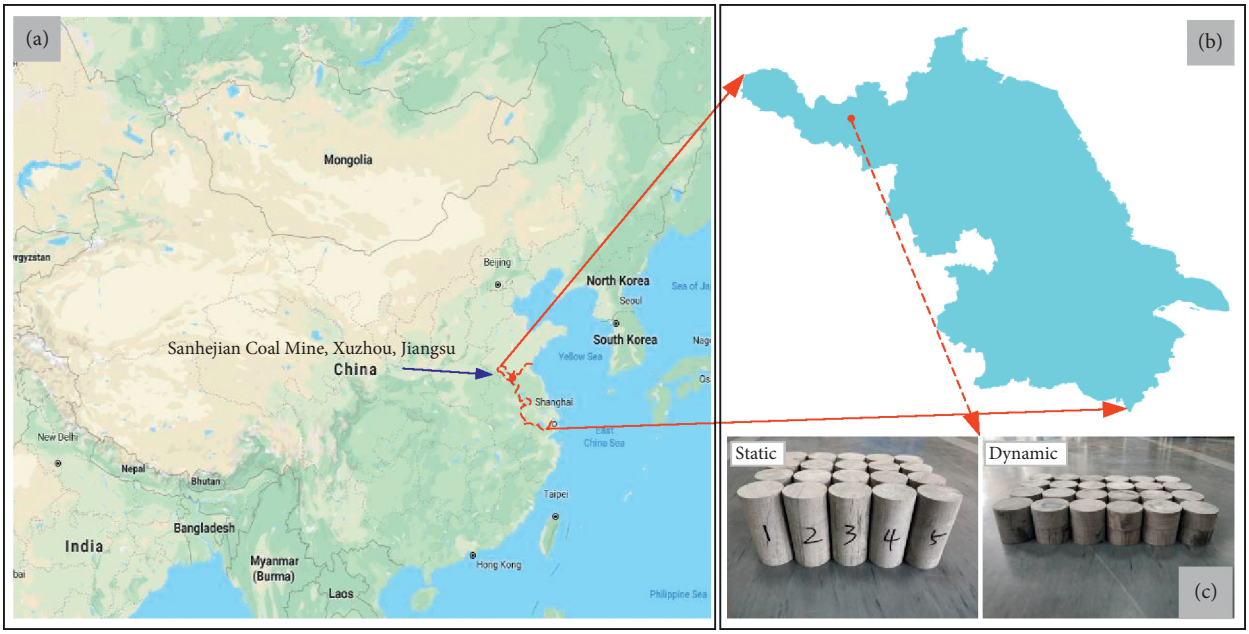

Figure 1: Location of the Jiangsu province from where the sandstone samples were obtained. (a) Location in China. (b) Detailed map of Jiangsu province. (c) The samples for static and dynamic tests; red point: rough location of Sanhejian Coal Mine.

Table 1: Several methods for calculating rock brittleness.

Methods	Equation	Remarks	Reference
Mineral composition	$BI_1 = v_{Qtz}/v_{Qtz+Cl+Cb}$ $BI_2 = v_{Qtz+Cb}/v_{Qtz+Cb+Toc+Cl}$	v is the fraction of brittle/ductile mineral; Qtz, Cl, Cb, and Toc are the quartz, clay carbonates, and total organic carbon, respectively	[14] [11]
Strain	$BI_3 = \varepsilon_e/\varepsilon_p$ $BI_4 = (\varepsilon_r - \varepsilon_p)/\varepsilon_p$	e, p, and r are the total elastic strain, failure strain, and residual strain, respectively	[22] [23]
Stress	$BI_5 = (\sigma_p - \sigma_r)/\sigma_p$ $BI_6 = \sigma_r/\sigma_p$	p and r are the peak stress and residual stress	[24] [25]
Rock strength	$BI_7 = \sigma_u/\sigma_t$ $BI_8 = (\sigma_u - \sigma_t)/(\sigma_t + \sigma_t)$	u denotes uniaxial compressive strength; t is the tensile strength	[26] [22]
Energy balance	$BI_9 = dw_{et}/(dw_p + dw_r)$ $BI_{10} = dw_a/(dw_e + dw_p)$	dw_{et} is the total elastic energy; dw_p is the plastic energy; dw_r is the rupture energy;dw_a is the postpeak addition energy; and dw_e is the consumed elastic energy	[27] [5]

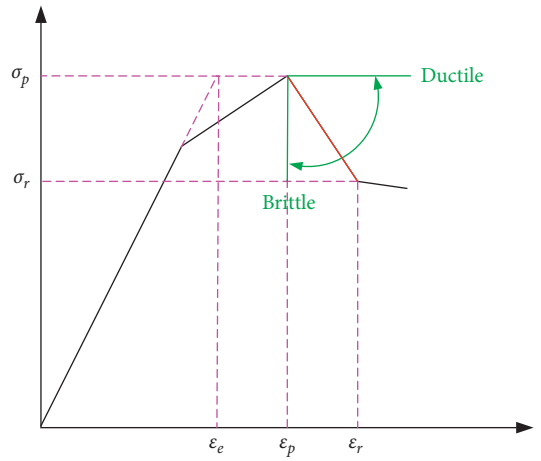

Figure 2: The stress-strain relationship of typical rock materials.

microstructure and stress state leads to the change of rock brittleness [28]. In order to simplify simulating the above process, we carried out freeze-thaw tests on the selected samples. This is because the freeze-thaw process leads to significant changes in the microstructure of rock resulting in irreversible structural damage of rock [29]. Moreover, the cyclic freeze-thaw action also has a clear effect on rock brittleness [16]. Here, it is worth emphasizing that the temperature treatment (freeze-thaw) is only used to control the brittleness of the test samples.

As shown in Figure 3, after the temperature treatment, there were significant changes in the stress-strain curves of the test sample, such as an increase in the prepeak plastic phase and a shift in the slope after the peak point, indicating the variation in the brittleness of the tested samples. Also, the brittleness indexes BI_3 and BI_5 were determined from the stress-strain curves, as shown in Figure 4. From the stress-strain curves, it is clear that the testing samples can be considered as completely brittle when they are not affected by temperature treatment, namely, illustrating that both BI_3 and BI_5 are 1. With the temperature treatment, the BI_3 and BI_5 showed a linearly decreasing trend, suggesting a decrease in the brittleness of the samples. It is worth noting that since BI_3 and BI_5 have the same varying behavior, for simplicity, BI_3 was used as the index for evaluating brittleness in this paper.

2.3. Dynamic Tests. In this study, the dynamic impact compression tests recommended by ISRM were carried out using a split Hopkinson pressure bar (SHPB) system (50 mm diameter) developed by Central South University. As shown in Figure 5, the SHBP system is composed of an incident bar, a transmitted bar, an absorption bar, and damper bar. All of the bars are made of high-strength 40Cr alloy steel with an elastic modulus, density, and P-wave velocity of 230 GPa, 7.821 g/m^3, and 5462 m/s, respectively. Before the tests, a coupling agent (Vaseline) was evenly smeared on the end-faces of the sample and the bars to reduce the end-friction effects [21].

It is a precondition for a valid dynamic impact compression test that the rock sample is assumed to be in stress equilibrium. In other words, the dynamic stress on both ends of the sample should be roughly the same. The stress balance at the two ends of the sample can be determined by the relationship between the incident (In) wave, reflected (Re) wave, and transmitted (Tr) wave. As shown in Figure 6, the samples reached dynamic stress equilibrium in this study. Another assumption is that of one-dimensional stress wave propagation; that is, that stress waves propagate along the bars in one dimension at all times.

2.4. Macrofracturing/Microfracturing in Rocks. To study the effect of sample brittleness on macroscopic failure modes and microscopic fracture morphology at the dynamic loading conditions, a high-speed camera and scanning electron microscope (SEM) equipment were used in this study (see Figure 5). The microscopic morphological characteristics of the sample after testing were studied using SEM, and the fracture evolution of the sample during the loading process was monitored by a high-speed camera.

3. Experimental Results and Analysis

Based on the brittleness indexes determined in Section 2.2 (see Figure 4), the deformation behavior and macroscopic fracture characteristics of different brittle samples were investigated under different loading strain rates using the SHPB test system. Moreover, the effect of the variation in sample brittleness on the dynamic strength increase factor was also studied.

3.1. Effect on Dynamic Stress-Strain Behaviors. Following these two assumptions in Section 2.3, the stress σ, strain ε, and strain rate $\dot{\varepsilon}$ of the samples with loading time can be obtained by equation (2) [21]. Based on equation (2), Figure 7 presents the dynamic stress-strain curves of the samples with different loading strain rates and brittleness parameters.

$$\begin{cases} \sigma(t) = \dfrac{AE}{2A_s}\left[\varepsilon_I(t) + \varepsilon_R(t) + \varepsilon_T(t)\right], \\ \varepsilon(t) = \dfrac{C}{l_s}\displaystyle\int_0^t \left[\varepsilon_I(t) - \varepsilon_R(t) - \varepsilon_T(t)\right]\mathrm{d}t, \\ \dot{\varepsilon}(t) = \dfrac{C}{l_s}\left[\varepsilon_I(t) - \varepsilon_R(t) - \varepsilon_T(t)\right], \end{cases} \tag{2}$$

where $\sigma(t)$, $\varepsilon(t)$, and $\dot{\varepsilon}(t)$ represent the stress, strain, and strain rate of the samples at a certain moment, respectively. E, C, and A are the elastic modulus, P-wave velocity, and cross-sectional area of the elastic bars. l_s and A_s are the length and cross-sectional area of the specimen. $\varepsilon_{\mathrm{I}}(t)$, $\varepsilon_{\mathrm{R}}(t)$, and $\varepsilon_{\mathrm{T}}(t)$ represent incident strain, reflected strain, and transmitted strain of the bars at a certain moment, respectively.

Figure 7(a) shows the influence of strain rate effect on the stress-strain behavior of the tested sample at a static brittleness index of 0.73, and corresponding plots for the stress-strain curves at different brittleness indexes are presented in Figure 7(b). As seen in Figure 7(a), the prepeak yield phase of the dynamic stress-strain curves varies significantly by the loading strain rate. The yield phase before the prepeak gradually decreases with increasing loading strain rate, indicating the extent of plastic deformation is affected by the strain rate and tends to decline as the strain rate increases. On the other hand, the smaller the plastic deformation, the less energy dissipated before the peak point, and the more stored elastic energy, the more likely to brittle failure after the peak point [5]. Moreover, the sandstone samples first exhibit type I failure behavior and then Type II failure behavior in the postpeak phase, and the test results were consistent with the results of other previous works [16, 26], which signifies that the sandstone samples transform from ductile to brittle failure during the rupture process. At the

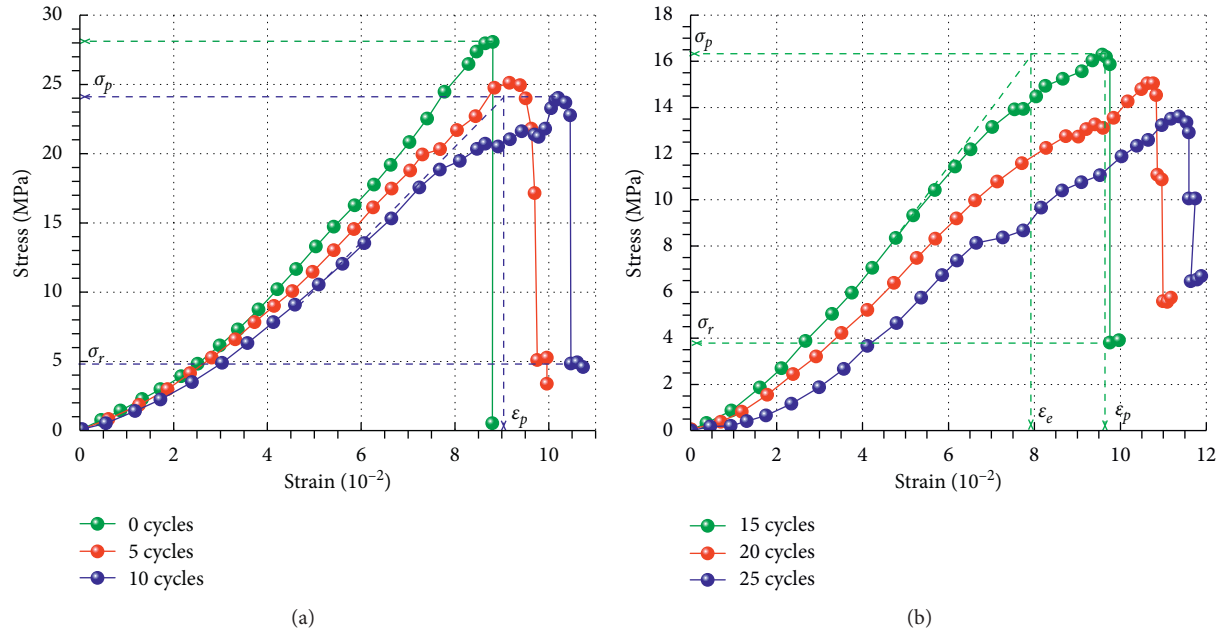

Figure 3: Stress-strain curves of the samples subjected to different freeze-thaw action.

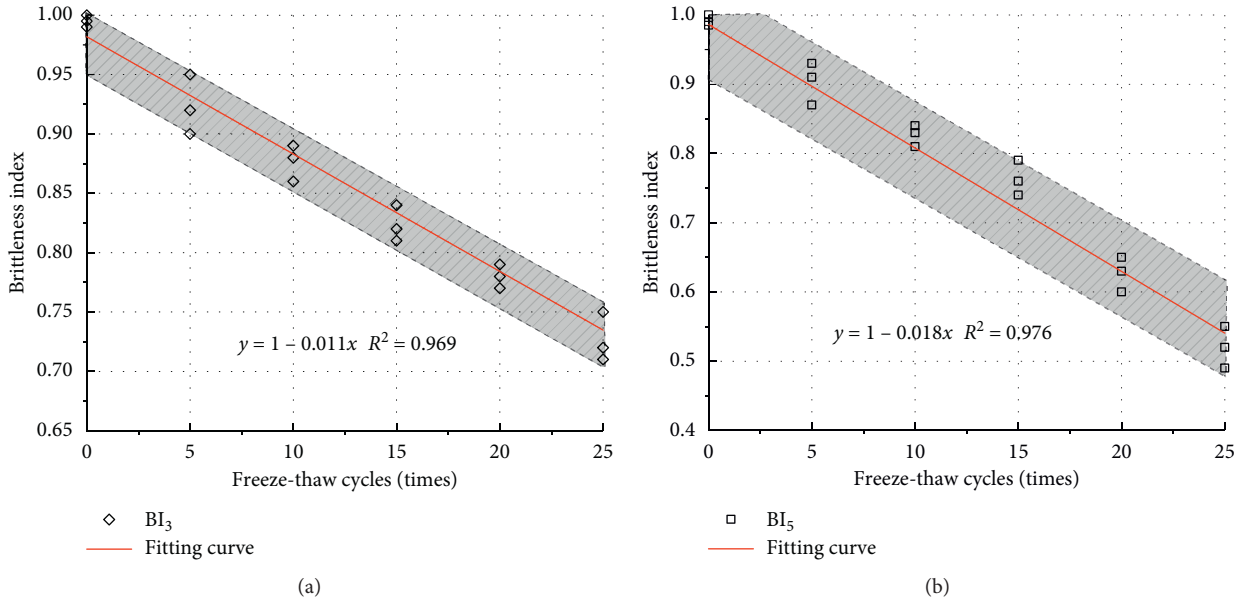

Figure 4: The changes in brittleness parameters of the tested samples.

same time, this shift in postpeak behavior reflects a change in the sample failure process from one that requires external energy to self-sustaining failure, which is a characteristic of type II failure. This phenomenon also demonstrates that, at high strain rates, the elastic energy accumulated within the sandstone is sufficient to sustain the failure process of the sample [9].

In Figure 7(b), the brittleness of the tested sample has a significant effect on the dynamic stress-strain curves at the same loading strain rate. As the sample brittleness under static loading increases, the prepeak yield phase of the dynamic stress-strain curve of the sample tends to decline. This implies that the sample brittleness under dynamic loading is still subject to a relationship with the brittleness under static loading. Also, after the peak point, there is a clear shift in the failure process of the sample from type I to type II. For example, when the brittleness index under static loading is above 0.82, the postpeak stress-strain curves display an apparent type I failure process, while when the brittleness index is less than 0.82, the failure behavior gradually transforms into the type II failure, which means that the samples with a lower brittleness index under static

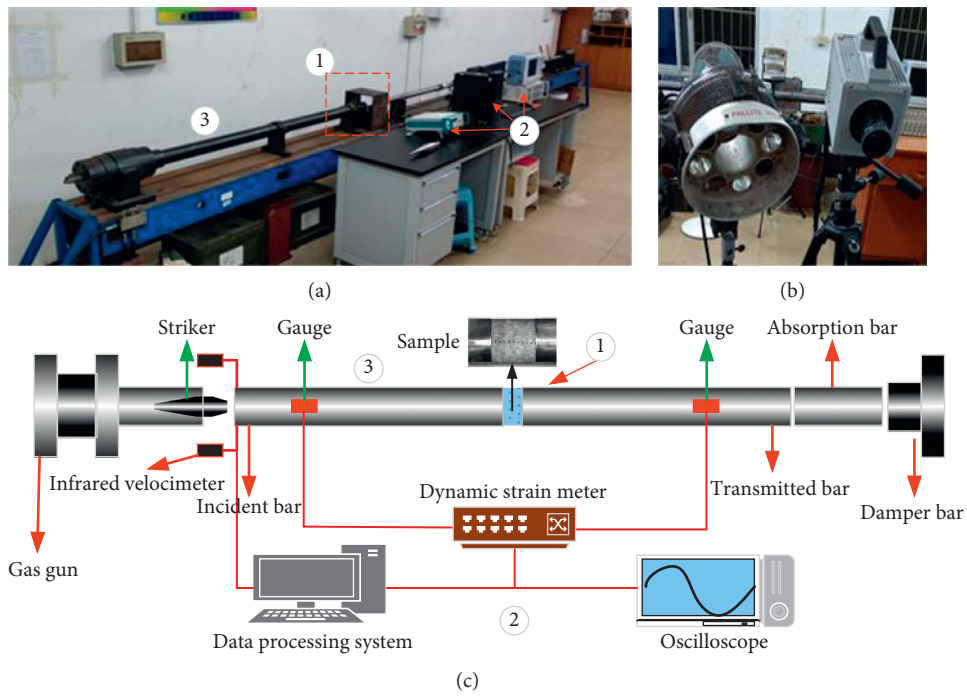

Figure 5: The split Hopkinson pressure bar test system. (a) SHPB device. (b) High-speed camera. (c) Schematic diagram.

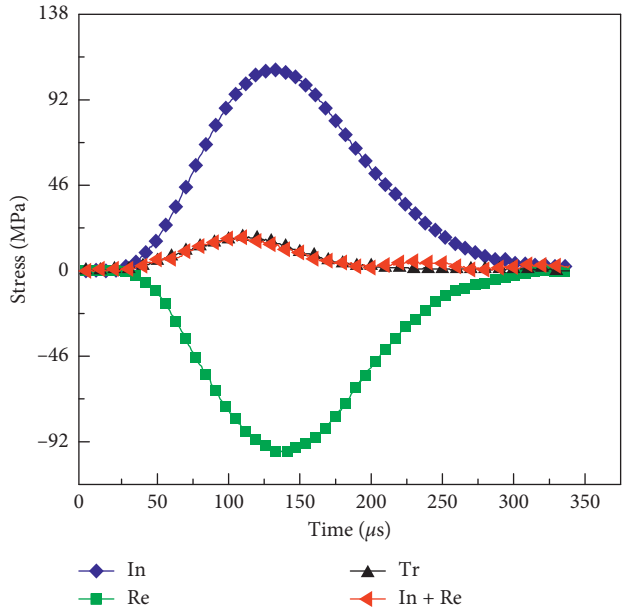

Figure 6: The verification of stress equilibrium in dynamical test (In, Re, and Tr refer to incident, reflected, and transmitted waves, respectively).

loading are more susceptible to self-sustaining failure after the peak point under dynamic loading. That is, the reduction of brittleness under dynamic loading often leads to the sudden brittle destruction of the rock samples in the postpeak stage.

Furthermore, based on the dynamic stress-strain curves, the brittleness indexes under dynamic loading are calculated in Figure 8. As presented in Figure 8(a), the brittleness index of the sample shows an increasing trend with the strain rate under dynamic loading. A linear function was adopted as the best function for variation of sample brittleness. For instance, the brittleness index under impact conditions increases from 0.82 to 0.89 as the loading strain rate increases from 63 s^{-1} to 156 s^{-1}, indicating that with increasing loading strain rate, the postpeak failure process of the sample exhibits more pronounced brittleness and more susceptibility to sudden destabilization. Also, Figure 8(b) plots the variation in dynamic brittleness index versus static brittleness index at a loading strain rate of 63 s^{-1}. As seen, the brittleness index of the sample is influenced by the loading strain rate and exhibits more pronounced brittleness. At a brittleness index of 0.73 under static loading, the brittleness index increases by 0.05 to 0.78 under dynamic loading, while at a brittleness index of 0.82 under static loading, the incremental value reaches 0.06 under dynamic loading. Besides, under the same loading strain rate, the brittleness index under dynamic loading responds linearly to the brittleness index under static loading with a growth slope greater than 1; that is, the brittleness index under dynamic loading is greater than under static loading, and the increasing value is positively correlated with the brittleness index under static loading.

Additionally, the dynamic strength increase factor of the tested sample is calculated for different strain rates and brittleness indexes based on equation (3), as shown in Figure 9. It can be observed that as the brittleness index declines, the dynamic strength increase factor displays an increasing trend. For example, when the loading strain rate is 92 s^{-1}, the corresponding dynamic strength increase factor decreases from 8.84 to 7.03 as the brittleness index increases from 0.73 to 0.86. Here, it should be noted that the dynamic strength increase factor in Figure 9 is cumulative values.

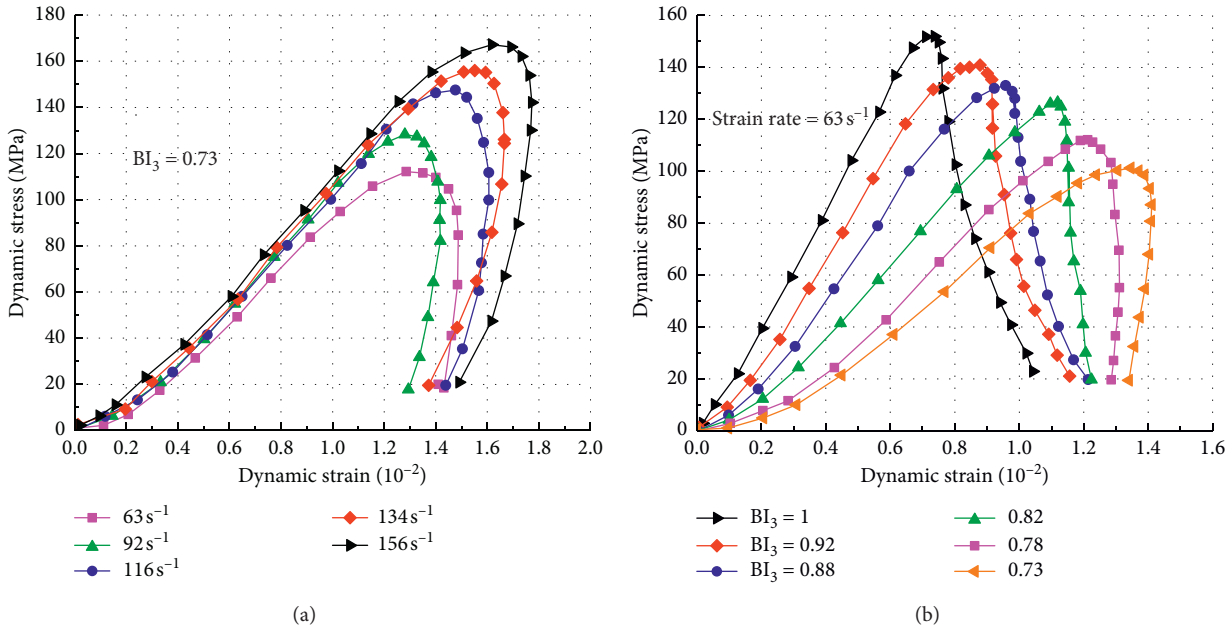

Figure 7: Dynamic stress-strain curves of the samples. (a) At the same brittleness condition. (b) At the same loading strain rate.

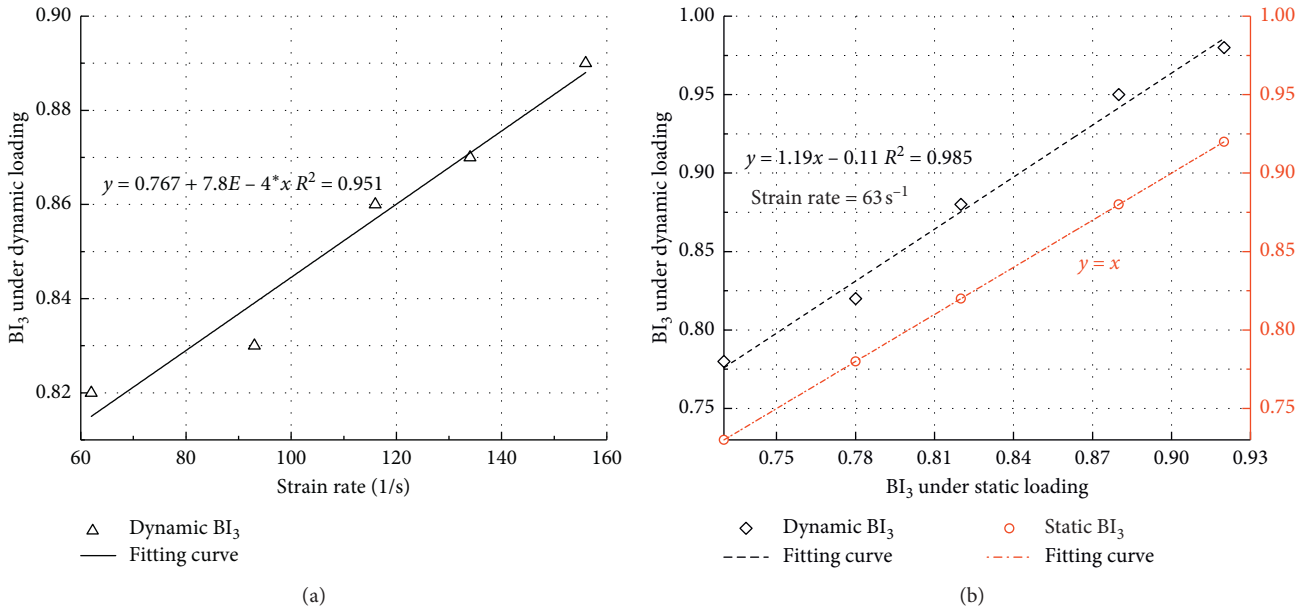

Figure 8: The variation in brittleness index BI_3. (a) Effect of strain rate on BI_3. (b) Relationship of brittleness index under different loading conditions.

Moreover, the dynamic strength increase factors present a significant increasing trend as the loading strain rate increases. Also, the dotted line in the figure illustrates that the dynamic strength increase factor is jointly influenced by brittleness and loading strain rate and is negatively correlated with brittleness, while it is positively correlated with strain rate. In addition, the relationship between the strength increase factor and the brittleness index at different strain rates was fitted, as shown in equation (4). The reduction in the sample brittleness leads to an increase in the dynamic strength increase factor, signifying an increase in the internal accumulated energy during the impact loading, and thus the postpeak process is more likely to suffer a brittle failure, which is consistent with what is shown in Figure 7(b).

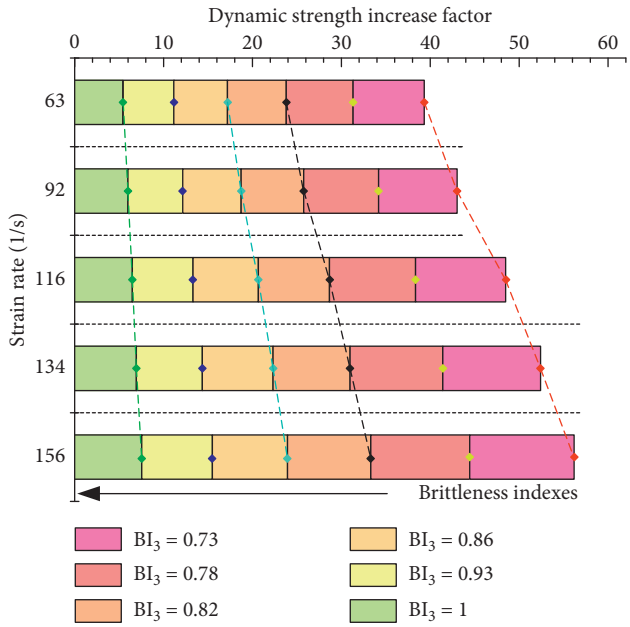

Figure 9: The evolution of dynamic strength increase factor with the brittleness and loading strain rates.

$$c = \frac{f_b(\dot{\varepsilon}) - f_b(s)}{f_b(s)}, \tag{3}$$

where $f_b(\dot{\varepsilon})$ is the peak strength of the sample at a certain brittleness b; $\dot{\varepsilon}$ refers to the strain rate under dynamic loading; and $f_b(s)$ is the static peak strength of the sample.

$$\begin{cases} c = 21.8 - 19.3 * b; \\ R^2 = 0.852\left(156\,\mathrm{s}^{-1}\right), \\ c = 20.7 - 18.4 * b; \\ R^2 = 0.864\left(134\,\mathrm{s}^{-1}\right), \\ c = 18.1 - 16.9 * b; \\ R^2 = 0.850\left(116\,\mathrm{s}^{-1}\right), \\ c = 14.7 - 13.4 * b; \\ R^2 = 0.818\left(92\,\mathrm{s}^{-1}\right), \\ c = 13.6 - 10.5 * b; \\ R^2 = 0.885\left(63\,\mathrm{s}^{-1}\right), \end{cases} \tag{4}$$

where c refers to the dynamic strength increase factor; b is the sample brittleness.

3.2. Effect on Macrofracture. As shown in Figure 10, a high-speed camera with the 80,000 frame rate is employed to capture the dynamic compression process of the sample under different conditions, where 1 is the initial state of the sample, 2 is the compression state, 3 is the destruction state, and 4 is the degree of axial compression before the failure of the testing sample. From Figures 10(a) and 10(b), the compression and failure modes of the sample are closely related to the brittleness at a loading strain rate of 134 s^{-1}: when the brittleness index is 0.88, the sample is significantly damaged under the dynamic loading, mainly in the form of split failure with a small number of shear cracks, and the failure cracks penetrate the whole sample. In contrast, when the brittleness decreases ($BI_3 = 0.73$), the fracture form of the sample transitions from a large fracture degree split failure with multiple cracks to a small fracture degree split-shear failure with few cracks, indicating a decrease in the brittleness of the sample under dynamic loading. At the same time, a significant variation in the extent of sample compression can be observed, showing an increasing trend with decreasing brittleness, while when the strain rate is reduced (see Figure 10(c)), the failure mode and compression degree of the sample are significantly changed under dynamic loading, and the failure modes change from a split failure to a shear failure, showing a weaker extent of rupture compared with Figure 10(b). Moreover, the axial compression displacement of the testing sample increases, indicating a large deformation during dynamic impact consistent with the results shown in Figure 7(b). Overall, the test results show that with the decrease of strain rate, the sample failure mode changes from split failure to shear failure, presenting a decline of the brittleness under dynamic loading, and the decrease of brittleness index also leads to the transition of the sample from split failure mode to shear split failure mode.

3.3. Effect on Micromorphology. The micromorphological changes in the sandstone samples under different loading strain rates and brittleness conditions are inferred using the scanning electron microscope (SEM) images, as shown in Figure 11. The image results show that the brittleness and strain rate have a significant effect on the surface morphology of the studied sandstone sample. When the loading strain rate is constant, the surface morphology of the sample gradually transforms from rough to smooth with the increase of brittleness. In addition, it is obvious that the number of microcracks on the fracture surface also presents an increasing trend. This can be attributed to the fact that as the brittleness increases, the crack bifurcation or branching decreases, leading to the surface morphological transformation [19]. Indeed, the internal microcracks development is closely related to the prepeak dissipation energy, while it is known from the stress-strain curves (see Figure 7) that as the brittleness increases, the prepeak dissipation energy decreases, and the corresponding energy required for microcracks development reduces, which can explain the changes in the microscopic surface morphology of the sample. Furthermore, as the brittleness of the samples is constant, the roughness of the sample surface has significant variations with the increase of the strain rate. For example, as the loading strain rate is 63 s^{-1}, the microscopic morphology of the fracture surface is smooth with less mineral particles and debris attached, while when the loading strain rate increases to 156 s^{-1}, the surface of

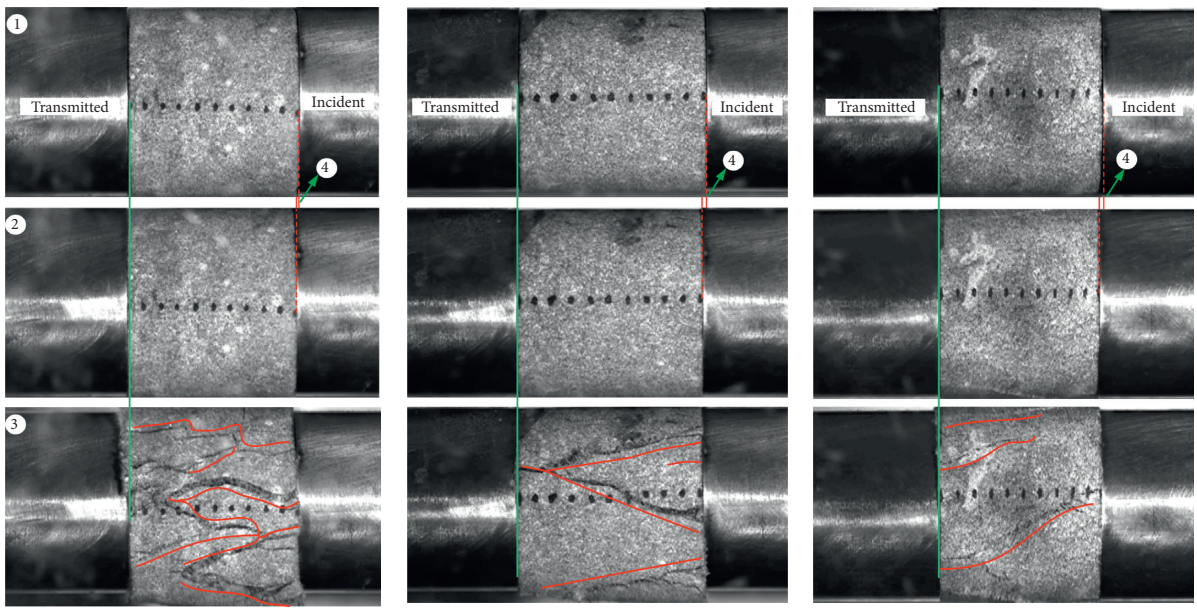

Figure 10: Effect of different brittleness and loading strain rates on the macroscopic failure modes of the testing samples. (a, b) The dynamic failure process of samples with brittleness index of 0.88 and 0.73 at a loading strain rate of 134 s^{-1}, respectively. (c) The dynamic failure process of the sample with a brittleness index of 0.73 at a loading strain rate of 93 s^{-1}. (a) $BI_3 = 0.88$; $\dot{\varepsilon} = 134\ s^{-1}$. (b) $BI_3 = 0.73$; $\dot{\varepsilon} = 134\ s^{-1}$. (c) $BI_3 = 0.73$; $\dot{\varepsilon} = 93\ s^{-1}$.

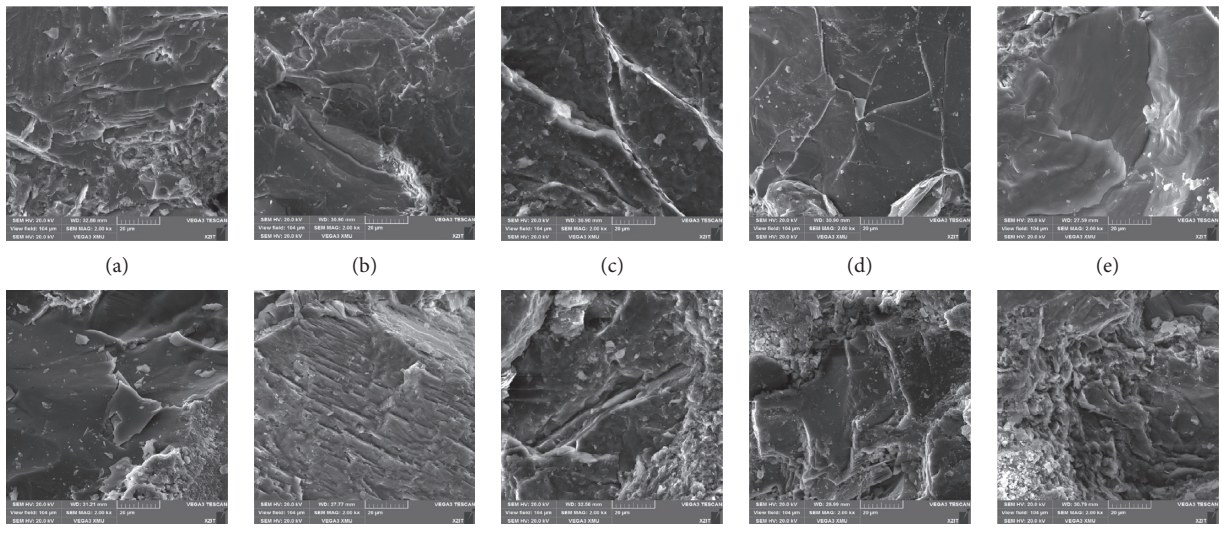

Figure 11: The SEM images under different brittleness and loading strain rate conditions (2000 times). (a)$\dot{\varepsilon} = 63\ s^{-1}$; $BI_3 = 0.77$. (b)$\dot{\varepsilon} = 63\ s^{-1}$; $BI_3 = 0.81$. (c)$\dot{\varepsilon} = 63\ s^{-1}$; $BI_3 = 0.86$. (d)$\dot{\varepsilon} = 63\ s^{-1}$; $BI_3 = 0.92$. (e)$\dot{\varepsilon} = 63\ s^{-1}$; $BI_3 = 1$. (f)$\dot{\varepsilon} = 63\ s^{-1}$; $BI_3 = 0.82$. (g)$\dot{\varepsilon} = 92\ s^{-1}$; $BI_3 = 0.82$. (h)$\dot{\varepsilon} = 116\ s^{-1}$; $BI_3 = 0.82$. (i)$\dot{\varepsilon} = 134\ s^{-1}$; $BI_3 = 0.82$. (j)$\dot{\varepsilon} = 156\ s^{-1}$; $BI_3 = 0.82$.

the samples is rough, accompanied by a large number of mineral particles and debris. The onset of this phenomenon is associated with an increase in strain rate and can be explained by an increase in crack branching or branching in dynamic rock fractures as the loading rate increases.

4. Discussions

Unlike some mechanical parameters, such as elastic modulus and Poisson's ratio that reflect only a single aspect of the rock mechanical behavior, brittleness is a comprehensive

description of the rock mechanical properties. Usually, brittleness values are obtained as relative brittleness values measured under certain loading conditions and related to the experimental conditions and properties of the rock materials such as size, nonhomogeneity, and anisotropy. Zhu and Tang concluded that rocks exhibiting brittleness under static loading are significantly different from those under dynamic loading conditions [30]. This variability is shown in Figures 7 and 8, especially the gradual transition from type I to type II in postpeak failure behavior under dynamic loading, and Ai et al. suggested that this transition in failure types demonstrates that the rocks yielded self-sustaining failure [5]. Using indoor experimental results, Zhang et al. pointed out that the brittle variation under static loading affects the postpeak mechanical behavior of rocks under dynamic loading [16]. Figure 7(b) shows that the variation in brittleness under static loading affects the deformation and failure behavior of the rocks under dynamic loading, and it can be seen that the decreasing brittleness leads to an increase in the prepeak plastic phase and the emergence of the postpeak self-sustaining failure behavior under the dynamic loading. The brittleness is also affected by the loading strain rate, showing a linear increasing trend. Moreover, Nejati and Ghazvinian studied the fracture surface morphology of different brittle rocks and found that brittleness affects the rock failure surface and the dynamic failure surface is rougher than the static failure surface [19]. However, as the brittleness of the sample increases, the failure surface becomes progressively smoother, while the increase in strain rate shows the opposite results (see Figure 11). In addition, the changes in brittleness affect the macroscopic failure mode of rock materials under dynamic loading from split failure with multicracks to shear failure with fewer cracks, and the results of this study coincide with those of Chen et al. [1].

5. Conclusions

As a primary issue in rock engineering, brittleness is an essential property of rocks closely related to prepeak and postpeak failure behaviors. In this paper, we study the effect of variation of brittleness on the mechanical behavior of coal measures sandstone in the Sanhejian Coal Mine under dynamic loading. In addition, a high-speed camera and scanning electron microscope (SEM) are also combined to analyze the effect of brittleness on the macro-/microscopic failure mode of the sample. The main conclusions are as follows:

(1) As the dynamic loading strain rate increases, the brittleness index of the samples increases linearly with the loading strain rate. When the loading strain rate increases from 63 s^{-1} to 156 s^{-1}, the yield phase of the dynamic stress-strain curves decreases significantly, and the brittleness index increases from 0.82 to 0.89.

(2) The brittleness index under dynamic impact loading is greater than that under static loading of the sample. Also, the postpeak behavior of the dynamic stress-strain curves is influenced by the static brittleness index. When the dynamic loading strain rate is 63 s^{-1}, the postpeak behavior of the dynamic curve transitions from type I to type II failure mode with self-sustaining failure.

(3) The macroscopic failure mode and microscopic fracture morphology of the samples are both affected by the rock brittleness. With the decrease of brittleness, the macroscopic failure mode of the sample changes from split failure to shear failure, and the number of cracks decreases. Besides, the microscopic fracture morphology gradually became rougher from smooth.

Data Availability

The data used to support the findings of this study are available from the corresponding author upon request.

Conflicts of Interest

The authors declare that there are no conflicts of interest regarding the publication of this paper.

Acknowledgments

This work was supported by the National Natural Science Foundation of China (U1803118, 51974296, 52061135111, and 41931284).

References

[1] G. Chen, W. Jiang, X. Sun, C. Zhao, and C. A. Qin, "Quantitative evaluation of rock brittleness based on crack initiation stress and complete stress-strain curves," *Bulletin of Engineering Geology and the Environment*, vol. 78, no. 8, pp. 5919–5936, 2019.

[2] B. G. Tarasov and T. R. Stacey, "Features of the energy balance and fragmentation mechanisms at spontaneous failure of class I and class II rocks," *Rock Mechanics and Rock Engineering*, vol. 50, no. 10, pp. 2563–2584, 2017.

[3] S. Aligholi, G. R. Lashkaripour, and M. Ghafoori, "Strength/brittleness classification of igneous intact rocks based on basic physical and dynamic properties," *Rock Mechanics and Rock Engineering*, vol. 50, no. 1, pp. 45–65, 2017.

[4] Y. Xia, H. Zhou, C. Zhang, S. He, Y. Gao, and P. Wang, "The evaluation of rock brittleness and its application: a review study," *European Journal of Environmental and Civil Engineering*, vol. 23, pp. 1–41, 2019.

[5] C. Ai, J. Zhang, Y.-w. Li, J. Zeng, X.-l. Yang, and J.-g. Wang, "Estimation criteria for rock brittleness based on energy analysis during the rupturing process," *Rock Mechanics and Rock Engineering*, vol. 49, no. 12, pp. 4681–4698, 2016.

[6] B. Du, H. Bai, M. Zhai, and S. He, "Experimental study on dynamic compression characteristics of red sandstone under wetting-drying cycles," *Advances in Civil Engineering*, vol. 2020, Article ID 6688202, 10 pages, 2020.

[7] X. Ou, X. Zhang, H. Feng, C. Zhang, X. Zhou, and L. Wang, "Static and dynamic Brazilian tests on layered slate considering the bedding directivity," *Advances in Civil Engineering*, vol. 2020, Article ID 8860558, 11 pages, 2020.

[8] J. Jiang, D. Wang, X. Han, and S. Di, "Relationship between brittleness index and crack initiation stress ratio for different rock types," *Advances in Civil Engineering*, vol. 2020, Article ID 8091895, 12 pages, 2020.

[9] T. Wen, H. Tang, and Y. Wang, "Brittleness evaluation based on the energy evolution throughout the failure process of rocks," *Journal of Petroleum Science and Engineering*, vol. 194, Article ID 107361, 2020.

[10] D. M. Jarvie, R. J. Hill, T. E. Ruble, and R. M. Pollastro, "Unconventional shale-gas systems: the Mississippian Barnett Shale of north-central Texas as one model for thermogenic shale-gas assessment," *AAPG Bulletin*, vol. 91, no. 4, pp. 475–499, 2007.

[11] R. Rickman, M. V. Mullen, J. E. Petre, W. V. Grieser, and D. Kundert, "A practical use of shale petrophysics for stimulation design optimization: all shale plays are not clones of the Barnett Shale," in *Proceedings of the SPE Annual Technical Conference and Exhibition*, September 2008, Article ID SPE-115258.

[12] X. Jin, S. N. Shah, J.-C. Roegiers, and B. Zhang, "An integrated petrophysics and geomechanics approach for fracability evaluation in shale reservoirs," *SPE Journal*, vol. 20, no. 3, pp. 518–526, 2015.

[13] E. Rybacki, T. Meier, and G. Dresen, "What controls the mechanical properties of shale rocks?—part II: brittleness," *Journal of Petroleum Science and Engineering*, vol. 144, pp. 39–58, 2016.

[14] Y. J. Xia, L. C. Li, C. A. Tang, X. Y. Li, S. Ma, and M. Li, "A new method to evaluate rock mass brittleness based on stress-strain curves of class I," *Rock Mechanics and Rock Engineering*, vol. 50, no. 5, pp. 1123–1139, 2017.

[15] N. Li, Y. Zou, S. Zhang et al., "Rock brittleness evaluation based on energy dissipation under triaxial compression," *Journal of Petroleum Science and Engineering*, vol. 183, Article ID 106349, 2019.

[16] J. Zhang, H. Deng, J. Deng, and B. Ke, "Development of energy-based brittleness index for sandstone subjected to freeze-thaw cycles and impact loads," *IEEE Access*, vol. 6, pp. 48522–48530, 2018.

[17] T. Wen, H. Tang, Y. Wang, and J. Ma, "Evaluation of methods for determining rock brittleness under compression," *Journal of Natural Gas Science and Engineering*, vol. 78, Article ID 103321, 2020.

[18] M. Heidari, G. R. Khanlari, M. Torabi-Kaveh, S. Kargarian, and S. Saneie, "Effect of porosity on rock brittleness," *Rock Mechanics and Rock Engineering*, vol. 47, no. 2, pp. 785–790, 2014.

[19] H. R. Nejati and A. Ghazvinian, "Brittleness effect on rock fatigue damage evolution," *Rock Mechanics and Rock Engineering*, vol. 47, no. 5, pp. 1839–1848, 2014.

[20] F. Zhao, S. Qiang, and W. Zhang, "Quantitative analysis of the influence of temperature and confining pressure on brittleness of granite: a review," *Acta Geodynamica et Geomaterialia*, vol. 17, no. 1, pp. 39–50, 2020.

[21] F.-Q. Gong, X.-F. Si, X.-B. Li, and S.-Y. Wang, "Dynamic triaxial compression tests on sandstone at high strain rates and low confining pressures with split Hopkinson pressure bar," *International Journal of Rock Mechanics and Mining Sciences*, vol. 113, pp. 211–219, 2019.

[22] V. Hucka and B. Das, "Brittleness determination of rocks by different methods," *International Journal of Rock Mechanics and Mining Sciences & Geomechanics Abstracts*, vol. 11, no. 10, pp. 389–392, 1974.

[23] V. Hajiabdolmajid and P. Kaiser, "Brittleness of rock and stability assessment in hard rock tunneling," *Tunnelling and Underground Space Technology*, vol. 18, no. 1, pp. 35–48, 2003.

[24] R. Altindag, "Assessment of some brittleness indexes in rock-drilling efficiency," *Rock Mechanics and Rock Engineering*, vol. 43, no. 3, pp. 361–370, 2010.

[25] U. Smoltczyk and E. Gartung, "Geotechnical properties of a soft Keuper sandstone," in *Proceedings of the 4th Congress of ISRM*, vol. 2, pp. 639–644, Montreux, Switzerland, September 1979.

[26] R. Altindag, "The evaluation of rock brittleness concept on rotary blast hole drills," *Journal of the South African Institute of Mining and Metallurgy*, vol. 102, no. 1, pp. 61–66, 2002.

[27] B. Tarasov and Y. Potvin, "Universal criteria for rock brittleness estimation under triaxial compression," *International Journal of Rock Mechanics and Mining Sciences*, vol. 59, pp. 57–69, 2013.

[28] C. Zhou, K. Zhang, H. Wang, and Y. Xu, "A plastic strain based statistical damage model for brittle to ductile behaviour of rocks," *Geomechanics and Engineering*, vol. 21, no. 4, pp. 349–356, 2020.

[29] A. Momeni, Y. Abdilor, G. R. Khanlari, M. Heidari, and A. A. Sepahi, "The effect of freeze-thaw cycles on physical and mechanical properties of granitoid hard rocks," *Bulletin of Engineering Geology and the Environment*, vol. 75, no. 4, pp. 1649–1656, 2016.

[30] W. C. Zhu and C. A. Tang, "Numerical simulation of Brazilian disk rock failure under static and dynamic loading," *International Journal of Rock Mechanics and Mining Sciences*, vol. 43, no. 2, pp. 236–252, 2006.